

# Real-time observation of the optical Sagnac effect in ultrafast bidirectional fibre lasers

Cite as: APL Photonics 5, 016104 (2020); <https://doi.org/10.1063/1.5121723>

Submitted: 26 July 2019 . Accepted: 18 December 2019 . Published Online: 07 January 2020

M. Chernysheva , S. Sugavanam , and S. Turitsyn 



View Online



Export Citation



CrossMark

## ARTICLES YOU MAY BE INTERESTED IN

[Multimode nonlinear fiber optics, a spatiotemporal avenue](#)

APL Photonics 4, 110901 (2019); <https://doi.org/10.1063/1.5119434>

[Epitaxial quantum dot lasers on silicon with high thermal stability and strong resistance to optical feedback](#)

APL Photonics 5, 016103 (2020); <https://doi.org/10.1063/1.5120029>

[Creating and controlling complex light](#)

APL Photonics 4, 110806 (2019); <https://doi.org/10.1063/1.5132960>

APL Photonics  
Special Topic on Biomedical Photonics

READ NOW!

# Real-time observation of the optical Sagnac effect in ultrafast bidirectional fibre lasers

Cite as: APL Photon. 5, 016104 (2020); doi: 10.1063/1.5121723

Submitted: 26 July 2019 • Accepted: 18 December 2019 •

Published Online: 7 January 2020



View Online



Export Citation



CrossMark

M. Chernysheva,<sup>1,a)</sup> S. Sugavanam,<sup>2</sup> and S. Turitsyn<sup>2,b)</sup>

## AFFILIATIONS

<sup>1</sup>Leibniz Institute of Photonic Technology, Albert-Einstein Str. 9, Jena 07745, Germany

<sup>2</sup>Aston Institute of Photonic Technologies, Aston University, Aston Triangle, Birmingham B4 7ET, United Kingdom

<sup>a)</sup>Electronic mail: [maria.chernysheva@leibniz-ipht.de](mailto:maria.chernysheva@leibniz-ipht.de)

<sup>b)</sup>Also at: Novosibirsk State University, 2 Pirogova Str., Novosibirsk 630090, Russia.

## ABSTRACT

The optical Sagnac effect sets fundamentals of the operating principle for ring laser and fiber optic gyroscopes, which are preferred instruments for inertial guidance systems, seismology, and geodesy. Operating at both high bias stability and angular velocity resolutions demands special precautions like dithering or multimode operation to eliminate frequency lock-in or similar effects introduced due to synchronization of counterpropagating channels. Recently, to circumvent these limitations, ultrashort pulsed radiation was suggested to supersede conventional continuous wave operation. Despite the ultrafast nature of ultrashort pulse generation, the interrogation of the Sagnac effect relies on highly averaging measurement methods. Here, we demonstrate the novel approach to the optical Sagnac effect visualization by applying real-time spatio-temporal intensity processing and time-resolved spectral domain measurements of ultrashort pulse dynamics in rotating the bidirectional ring fiber laser cavity. Our results reveal the high potential of application of novel methods of optical Sagnac effect measurements, allowing enhancement of rotation sensitivity and resolution by several orders of magnitude.

© 2020 Author(s). All article content, except where otherwise noted, is licensed under a Creative Commons Attribution (CC BY) license (<http://creativecommons.org/licenses/by/4.0/>). <https://doi.org/10.1063/1.5121723>

## I. INTRODUCTION

Improving the accuracy of relative positioning or rotational sensing is important both for fundamental science and for various practical engineering applications. With progress in the general understanding of optical phenomena in a laser cavity and the development of advanced laser configurations came the ability to measure ultraslow angular velocities unlocking new breakthrough methods and approaches in this field. Thus, laser gyroscopes employing the optical Sagnac effect make it possible to detect rotations of the ground with a resolution of  $10^{-11}$  rad  $s^{-1}$  by integrating a signal over several hundreds of seconds.<sup>1,2</sup> Among the impressive recent applications, one can mention the direct observation of the rotational microseismic noise,<sup>3</sup> observation of Chandler and Annual wobbles,<sup>4</sup> and the detection of very long period geodetic effects on the Earth's rotation vector.<sup>4</sup> An alternative approach is pursued for self-navigation.<sup>5,6</sup> Here, the requirement of high data acquisition rates of a Sagnac phase shift of up to several kilohertz<sup>7</sup> is more critical

than rotation sensitivity. There is still much room for further development and performance improvement, for example, autonomous or driver-less cars require data acquisition rates much higher than the currently available tens of kilohertz<sup>5</sup> for precise vehicle positioning.

As mentioned above, the laser gyroscope technology is capable of providing highly sensitive and high-resolution measurements of the optical Sagnac effect. However, its application has both practical and fundamental limits and restrictions caused by their size, elaborate fabrication, maintenance, and, more importantly, by the impact of the frequency lock-in effect. Backscattered light enhances the coupling between counterpropagating beams, causing carrier frequency synchronization.<sup>8,9</sup> As a result, the beat note signal, manifesting the optical Sagnac effect, disappears for a range of small angular velocities.<sup>10</sup> Numerous approaches have been suggested to decrease backscattering, such as application of high-reflective dielectric coatings of cavity mirrors or external dithering or improvement of laser cavity geometry.<sup>9,10</sup> Owing to

the lock-in effect, maintenance-free all-fiber configurations, which are typically considered beneficial, become disadvantageous for laser gyroscopes as they suffer from Rayleigh scattering.<sup>11</sup> Alternative attempts for the frequency lock-in effect elimination have exploited ultrashort pulses instead of continuous wave radiation in laser gyroscopes,<sup>12,13</sup> since the counterpropagating ultrashort pulses interact only in two points in the cavity.<sup>14–16</sup> In such configurations, a differential phase shift of counterpropagating pulses due to the optical Sagnac effect is generally evaluated by the change in the interference pattern of two frequency combs, corresponding to counterpropagating ultrashort pulses at each round trip.<sup>17</sup>

To date, the interrogation of the optical Sagnac effect has relied on the study of its cumulative effect over time scales much larger than the typical cavity lifetime. Thus, existing methodologies impose a bottleneck on acquisition rates of the Sagnac phase shift, limiting it to a few kilohertz. The availability of ultrafast detectors and high-resolution real-time oscilloscopes has yielded a multitude of novel, real-time methodologies for studying ultrafast laser dynamics in both the intensity and spectral domains. For instance, the method of spatio-temporal dynamics<sup>18–20</sup> (see [supplementary material S1](#) for the detailed operational principle) makes it possible to identify specific features of interest in the laser output and to observe their evolution with round trip time resolution over several thousand round trips.<sup>21–24</sup> The Dispersive Fourier Transform (DFT)<sup>25–27</sup> (refer to [supplementary material S2](#) for the general operation concept) is a real-time spectral method that exploits the principle of Fraunhofer diffraction in the temporal domain and can be used to obtain the time-resolved spectra of successive mode-locked pulses.<sup>28–30</sup> This paper justifies such methods used to study the fast dynamics of counterpropagating ultrashort pulses and also open up perspectives for interrogating the optical Sagnac effect in real-time.

In this paper, we introduce a new concept of the optical Sagnac effect evaluation by analyzing the dynamics of a pair of counterpropagating ultrashort soliton pulses applying three real-time measurement techniques in a proof-of-principle demonstration bidirectional ultrafast fiber laser. First, we show how the real-time spatio-temporal dynamics of the counterpropagating pulses can

be used for direct observation and analysis of the temporal drift between solitons induced by the optical Sagnac effect accumulated over several round trips with a resolution of  $10^{-2}$  deg  $s^{-1}$ . Second, we show how such real-time measurements can be used to monitor angular velocities at a rate equivalent to the round trip time of the laser, resulting in effective acquisition rates that surpass current state-of-the-art commercially available modalities by at least two orders of magnitude. Third, we show how the synchronized regimes can be utilized for rotation sensing by employing real-time DFT measurements with a resolution of  $10^{-3}$  deg  $s^{-1}$ . All these techniques show great potential for improvement of the rotational resolution by orders of magnitude, while the initial findings show at least threefold resolution improvement, when compared to earlier demonstrated concepts of detecting the optical Sagnac effect using bidirectional ultrafast fiber lasers.<sup>16</sup> A simple theory based on a linear-regime approximation is presented, which helps to estimate the order of magnitude of resolution and errors of suggested methodologies and ascertain the appropriate strategy on tailoring laser parameters to achieve the requisite resolution.

## II. LASER DESIGN

Our experiments employ the hybrid mode-locked Erbium-doped fiber (EDF) laser setup (see Sec. V), placed on a rotating circular platform with a diameter of 0.62 m [Fig. 1(a)]. The angular velocities of the platform with an ultrafast laser can be varied from 0 to 0.3 deg  $s^{-1}$ . The stability of the ultrafast generation against nonlinear instabilities is ensured by a hybrid mechanism of passive mode-locking realized via single-walled carbon nanotube (SWNT) polymer saturable absorber and nonlinear polarization evolution (NPE). NPE relies on the section of the polarizing fiber with bow-tie geometry and allows tuning of the nonlinear transfer function, predefining the nature of interactions between counterpropagating pulses. The laser cavity comprises a 3-dB output coupler, which rotates with the entire interferometer cavity, creating the difference in the optical paths for counterpropagating pulses as reported for other simple Sagnac interferometers.<sup>31</sup> Afterwards, the counterpropagating pulses are

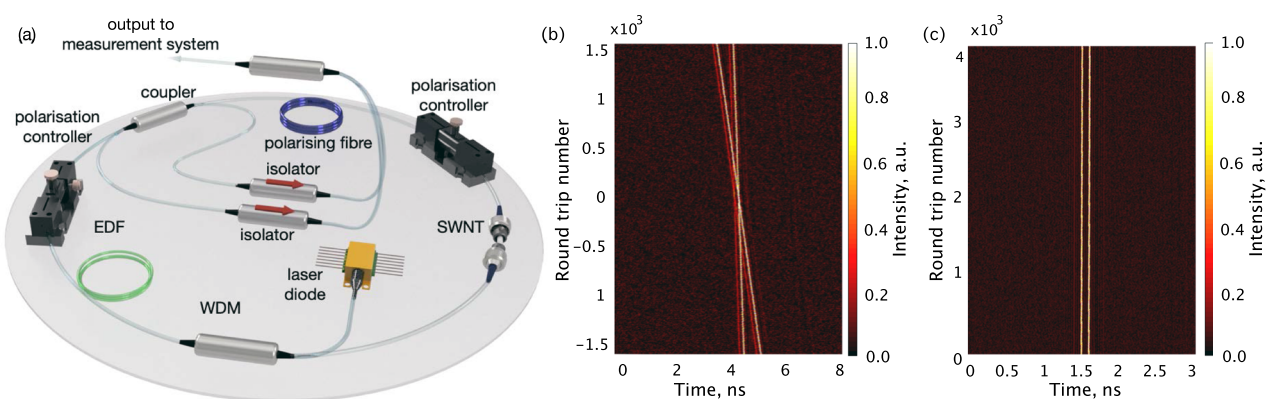


**FIG. 1.** The ultrafast bidirectional laser and its operational regimes. (a) Schematic setup of the ultrafast fiber laser used for optical Sagnac effect visualization. [(b) and (c)] Spatio-temporal dynamics of pulses with different (b) and synchronized repetition frequencies (c).

combined via a 3dB coupler, the output of which was used for real-time measurements.

The experiment showed that with proper tuning of the polarization state in the cavity, two stable bidirectional regimes can be achieved: when repetition rates of counterpropagating pulses differ by tens of hertz [Fig. 1(b)] and when pulses in both channels are generated at the same repetition rate of 14.78 MHz [Fig. 1(c)]. In the latter case, the lengths of ports of the coupler, combining counterpropagating pulses, were adjusted to achieve a pulse separation of  $\sim 100$  ps. We use different techniques for each of these two laser generation regimes to evaluate the optical Sagnac effect. The case of channels with different repetition rates has been analyzed by using spatio-temporal dynamics<sup>18,19,32</sup> (see [supplementary material 1](#)), and synchronized channels were measured with the DFT technique (see [supplementary material 2](#)).

### III. RESULTS

#### A. Time-domain analysis

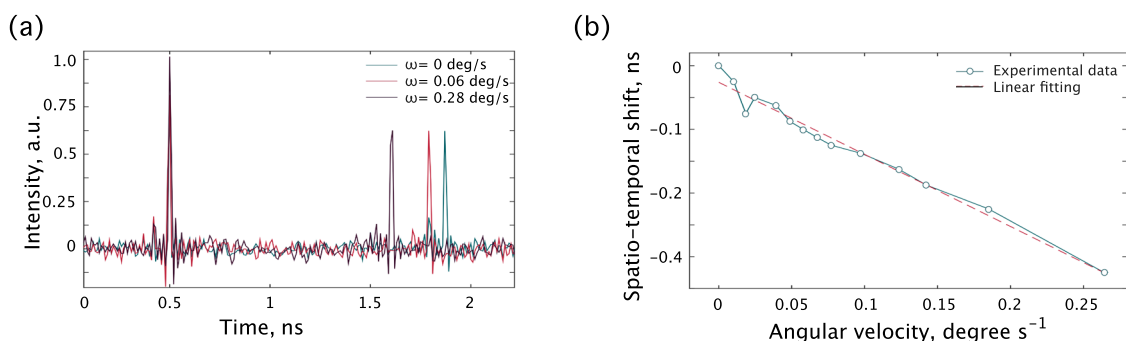
The methodology of spatio-temporal dynamics—that is, a two-dimensional representation of laser intensity evolution over round trips—makes it possible to observe round trip time-resolved dynamics of laser pulses (see [supplementary material S1](#)). Here, the bidirectional regime with different repetition frequencies of counterpropagating pulses will be considered. Figure 1(b) shows the spatio-temporal dynamics of the combined laser output over  $N_{RT} = 3000$  consecutive round trips, for the platform at rest. Since counterpropagating pulses are generated at slightly different repetition rates, their crossing point moves along the cavity over round trips. Thus, when combined at the output coupler, the trajectories of pulses present intersect, as the separation between pulses changes. The evolution traces for both pulses present straight lines, indicating that there are no uncompensated attractive or repulsive forces between counterpropagating pulses, which may affect their repetition rate. The trajectories cross when pulses overlap at the output coupler.

Figure 2(a) shows the relative positions of the counterpropagating pulses at the  $N_{RT} = 10^4$  round trip after their overlapping at different rotation velocities of the platform, showing that the rotation of the stage influences the cavity conditions for the pulses.

Figure 2(b) clearly shows the existence of a linear relation between the angular velocity and the corresponding relative pulse temporal drift. We attribute the deviations from the linear approximation to imperfections of the rotation stage, mainly owing to the slippage between the platform and the motor. The bidirectional laser operating in the nonsynchronized regime can be used for ascertaining not only the magnitude of the angular velocity but also the direction of rotation. Thus, Fig. 2(b) demonstrates the decrease in the pulse separation with the increase in the rotating velocity, while the stage rotating in the opposite direction will cause an increase in the pulse temporal separation.

The separation between the pulses with the laser platform in the rest condition [from Fig. 2(a)] was deducted from the actual measured values. Therefore, spatio-temporal shift at zero angular velocity is set to null in Fig. 2(b). The resulting difference between timing of arrival of clockwise (CW) and counter-clockwise (CCW) pulses at photodetector  $t_{CW} - t_{CCW}$  is introduced solely due to the optical Sagnac effect. The pulse separation at the 10<sup>4</sup>th round trip after pulses overlapping, thus, presents a monotonically decreasing function from zero to a minimum recorded value of  $\sim -0.45$  ns, owing to the direction of rotation of the stage. The error bars are not depicted, since the error of measurements (25 ps determined by the resolution of the measurement equipment) is smaller than the dot in the scatter plot.

The scale factor  $S$  of the Sagnac effect measurements for this particular configuration can be obtained directly from the slope of the linear fit in Fig. 2(b). Here, the scale factor is estimated to be  $0.885 \text{ deg s}^{-1}/\text{ns}$ . The resolution of measurements in this configuration can be attributed to the finite temporal resolution  $\delta t_{res}$  (here, 25 ps) and can be estimated as  $S \cdot \delta t_{res}$  to be  $22.12 \text{ mdeg s}^{-1}$  ( $386 \mu\text{rad s}^{-1}$ ). A theoretical estimate of the resolution can be obtained from well-known expressions for the optical Sagnac effect<sup>31</sup> [see Eq. (2) in Sec. V], as  $534.9 \mu\text{deg s}^{-1}$  ( $9.4 \mu\text{rad s}^{-1}$ ), which is much smaller than the experimentally obtained value. The differences can be attributed to the fact that the analytical expression Eq. (2) in Sec. V takes into account only the linear effects as brought about by the optical Sagnac effect, not considering attraction and repulsion introduced by the nonlinear effects across the laser cavity, similar to those observed in nonlinear loop mirrors,<sup>33,34</sup> and interaction in active media. Yet, the



**FIG. 2.** Observing the optical Sagnac effect in the time domain **when counterpropagating pulses are generated at different repetition rates.** (a) Temporal shift of combined pulses at three different angular velocities. (b) Pulse temporal shift due to the optical Sagnac effect (in reference to the platform at rest) at 10 000 round trips beyond the point of pulse overlapping.

experimental results show that there is a clear linear relationship between the angular velocity of the stage and the relative pulse separation, thus allowing us to use the current methodology for high accuracy angular velocity determination. The discussion on the scale factor stability in the current laser configuration is presented in [supplementary material 4](#). The resolution limit can be countered for a given laser configuration only by increasing the number of round trips— $N_{RT}$ . The slope of spatio-intensity trajectories of counterpropagating pulses in [Fig. 1\(b\)](#) shows that the temporal shift between pulse arrivals to the output coupler changes by 0.295 ps within one round trip time. Therefore, one can consider at least  $2.3 \times 10^5$  round trips after pulses coincide (for the platform at rest) before they overlap in the coupler again. Analysis of the entire dataset would make it possible to increase the resolution of the optical Sagnac effect measurements by more than one order of magnitude.

### B. Ultrafast measurements of the optical Sagnac effect

In the above, the cumulative temporal shift between counterpropagating pulses accrued after  $N_{RT} = 10^4$  round trips was used to visualize the cumulative optical Sagnac effect of the stage over the corresponding time period. One can obtain a measure of the angular velocity from a single-shot measurement, i.e., when  $N_{RT} = 1$  [see Eq. (2) in Sec. V]. While this method decreases the resolution of measurements by a factor of  $N_{RT}$ , it has the potential to increase the effective acquisition rate to the order of the cavity repetition frequency (hundreds of kilohertz to tens of megahertz), making it at least three orders of magnitude faster than measurement approaches applied in commercially available gyroscopes, even surpassing MEMS technologies.

[Figure 3\(a\)](#) shows the round trip resolved temporal separation  $\delta T_{N_{RT}}$  introduced between the clockwise and counterclockwise pulses. The temporal offset due to the difference in counterpropagating pulse repetition rates has been removed, leaving behind only the Sagnac effect induced temporal drift between the pulses. The plot indicates a linearly increasing separation between the pulses [[Fig. 3\(a\)](#)]. Thus, the average Sagnac temporal drift  $\langle \delta t_{Sagnac} \rangle$  over

each round trip can be obtained from the slope of the linear fit function [[Fig. 3\(a\)](#), dotted line]. Deviations about this linear fit  $\epsilon_{N_{RT}}$  can result from instantaneous drifts of the stage away from the mean angular velocity. [Figure 3\(b\)](#) shows the residuals of the linear fit, which are not  $\epsilon_{N_{RT}}$  but its cumulative sum up to the round trip  $N_{RT}$ —that is,  $\sum_{i=1}^{N_{RT}} \epsilon_{N_{RT}}$ .  $\epsilon_{N_{RT}}$  can thus be obtained from a simple first-order difference of the residuals of the linear fit [[Fig. 3\(c\)](#); also see [supplementary material 6](#)]. Thus, with knowledge of  $S$  and the instantaneous temporal drifts, the round trip time-resolved angular velocity measurements as shown in [Fig. 3\(c\)](#) (blue curve) can be obtained directly from time-domain spatio-temporal dynamics, via the formula

$$\Omega_N = S \cdot [\langle \delta t_{Sagnac} \rangle + \epsilon_N]. \quad (1)$$

We would like to stress that the increase in the acquisition rate always comes at the expense of the decrease in the measurement resolution by the same factor. Defining the final application will allow identification of suitable accuracy vs bandwidth trade-off. In principle, within the current measurement setup and laser configuration, while keeping the resolution of the Sagnac effect at a moderate value of  $94 \text{ mrad s}^{-1}$ , the acquisition rate can be as high as  $418 \times 10^3$  samples per second (or 418 kHz), calculated using Eq. (2) in Sec. V, using the value of the scale factor obtained in the linear approximation. However, as the scale factor in the experiment is drastically reduced owing to the nonlinear effects and interaction of counterpropagating pulses in the saturable absorber and active media, the bandwidth obtained in the experiment is closer to 19 kHz. The finite bandwidth effect has been taken into account in the above instantaneous angular velocity dynamics by incorporating a moving-window smoothing operation [orange curve, [Fig. 3\(c\)](#)]. While the angular velocity of our stage is currently limited to about  $0.2 \text{ deg s}^{-1}$ , the above methodology is not limited by the angular velocity. Actually, the presented methodology offers better resolution and therefore possibility to increase acquisition rates with high angular velocities and their large amplitude variations or oscillations. Such rotations introduce a greater temporal shift of the pulses, which will be easier to detect in regards of the finite temporal resolution of the real-time oscilloscope and photodetectors. Still, the

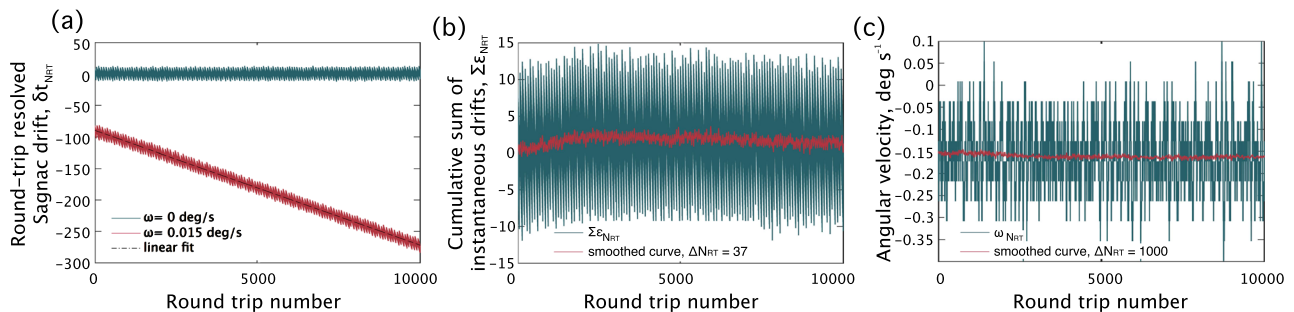


**FIG. 3.** Round trip time-resolved optical Sagnac effect measurements. (a) Temporal separation between clockwise and counterclockwise pulses for the stage at rest (blue curve) and in motion (orange curve). The black dashed line is a linear fit, indicative of constant angular velocity. (b) Blue curve—residual of the linear fit function, which is a cumulative sum  $\sum \epsilon_{N_{RT}}$  of the instantaneous deviations of the pulse separation over each round trip. The jagged appearance is a sampling artefact, which has been removed by a smoothing operation to give the orange curve. (c) Round trip resolved angular velocity obtained using Eq. (1), where  $\epsilon_{N_{RT}}$  is obtained from a first-order difference of the smoothed curve in (b). The orange curve here is again obtained by a smoothing operation to remove the sampling artefacts.

presented results demonstrate acquisition rates of an order of magnitude higher than current state-of-the-art and commercially available instruments.<sup>35,36</sup> We believe that the current ultrafast methodology, with the condition of further development of the fast electronics and decreasing its cost-metric parameters, will find application in the rapid developing area of automotive vehicles.<sup>5</sup>

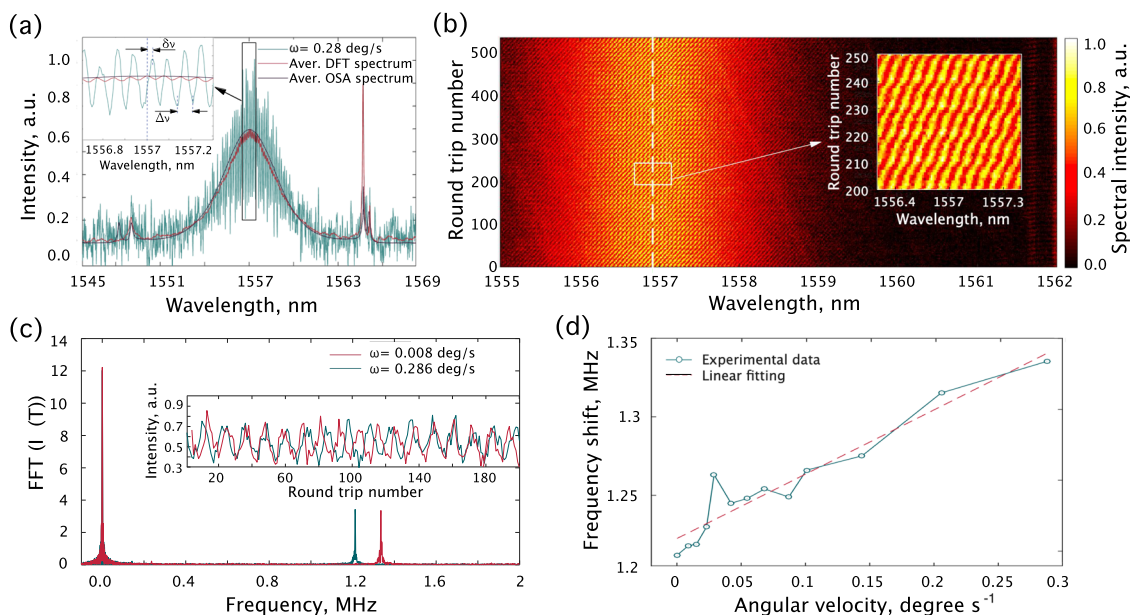
### C. DFT analysis

Figure 1(c) shows the second regime of operation of the bidirectional laser, where the clockwise and counterclockwise pulses have equal repetition rates, resulting in their observed parallel trajectories on the spatio-temporal dynamics. The length of output coupler fiber ports was chosen in such a way to ensure separation between counterpropagating pulses of  $\sim 100$  ps when combined [Figs. 1(c) and S3]. The synchronization of the pulse repetition rates of counterpropagating pulse trains is caused by the nature of colliding mode-locking.<sup>12,37</sup> The transition from the nonsynchronized mode described above to the pulse separation locked regime does not significantly modify the pulse parameters within experimental accuracy (see Fig. 5).

Analysis of the dynamics of the autocorrelation function over round trips for different rotation velocities of the platform with the laser (see supplementary material note S2) has proven that the separation of the pulses remains the same over 1000 s round trips regardless of the rotation velocity. Therefore, when such pulse repetition rate synchronization occurs, the influence of the Sagnac effect cannot be directly observed by using spatio-temporal intensity approaches, and one should proceed from the temporal domain to the spectral using the DFT technique.

The DFT technique has been implemented by propagating pulses through a spool of dispersion-compensation fiber with a total accumulated dispersion of  $-1200$  ps nm<sup>-1</sup>. Taking into account parameters of the measurement equipment used, i.e., photodiode and real-time oscilloscope, the electronic-based spectrum resolution of our system reaches 18 pm. Figure 4(a) demonstrates the highly modulated single-shot spectrum of a single pair of combined counterpropagating pulses due to their interference while they were stretched in dispersive media. The averaged single-shot spectrum over 5000 round trips [red curve in Fig. 4(a)] is in good agreement with the time-averaged spectrum recorded with the optical spectrum analyzer (OSA) for combined pulses (navy curve), and the position of characteristic Kelly side-bands correlates with one in individual spectra of counterpropagating pulses. It is known that the frequency of modulation of the spectral interference pattern is inversely related to the temporal separation  $t_{sep}$  of the pulses  $\Delta\nu = 1/t_{sep}$ .<sup>38</sup> In the previous scenario, the optical Sagnac effect introduces a change in the temporal separation, which should cause a change in the frequency of spectrum modulation. Here, however, the temporal separation between the pulses does not change with changing the angular velocity of the table, rendering the change in the frequency of spectral modulation unresolvable.

Figure 4(b) demonstrates recorded single-shot spectra over 5000 consecutive round trips. The Sagnac effect in this laser operation regime manifests in the form of a change in the tilt of the modulation pattern of the DFT spectrum [see inset in Fig. 4(b)]. To reveal the optical Sagnac effect, we can utilize the additional time scale available—that is, the evolution of the spectrum over round trips at a fixed wavelength. Here, we used  $\sim 1556.9$  nm shown as a white dashed line in Fig. 4(b). Figure 4(c) shows how the change in



**FIG. 4.** Optical Sagnac effect measurements by single-shot spectral evolution. (a) Single-shot spectrum, averaged single-shot spectra over  $N_{RT} = 5000$  round trips, and optical spectra, measured with the optical spectrum analyzer (OSA), of combined pulses. (b) Single-shot spectra dynamics within 500 round trips. Inset: zoomed-in central part of spectral evolution. (c) Frequency shift for two different angular velocities. Inset: spectral intensity fringing at  $\sim 1556.9$  nm—along the white dashed line in (b). (d) DFT response to different angular velocities.

the tilt is converted to a change in the frequency of spectral intensity modulation over round trips using the Fast Fourier Transform (FFT). Here, the FFT is accounted for the dynamics measured over 5000 round trips. The inset in Fig. 4(c) shows the round trip spectral intensity evolution for two angular velocities, measured along the white dashed line in Fig. 4(b).

The tilt in the spectral modulation when the platform is at rest appears due to initial differences in carrier frequencies of counterpropagating pulses, producing the carrier-envelope offset (CEO). The slope of the linear fit can then determine the scale factor of optical Sagnac effect measurements  $S_{DFT}$ , here  $17.2 \text{ mdeg s}^{-1}/\text{kHz}$ , with an error of  $(3 \text{ kHz})^{-1}$  (as set by the FFT resolution). The use of the DFT methodology allows resolution of the angular velocity of  $7.2 \text{ mdeg s}^{-1}$  ( $125 \mu\text{rad s}^{-1}$ ), while the theoretically predicted resolution according to Eq. (3) (see Sec. V) when  $N_{RT} = 5000$  is  $10 \mu\text{deg s}^{-1}$ . Here, the trade-off is a loss in temporal resolution of the angular velocity drift. The resolution can be enhanced via moving window FFTs or even higher-order windowing operations like the Wigner Ville distribution.<sup>32,39</sup> The resolution can be further enhanced by observing the intensity evolution over longer periods, here up to  $3.96 \times 10^5$  round trips. Therefore, the resolution is in principle limited by the oscilloscope memory.

#### IV. DISCUSSION AND CONCLUSION

To the best of our knowledge, this is the first demonstration of the application of real-time intensity and spectral domain approaches to measuring the optical Sagnac effect in a bidirectional ring ultrafast fiber laser. A direct time domain measurement of the Sagnac effect was just a decade ago considered as a low-accuracy signal processing method.<sup>40</sup> However, the advent of high-bandwidth detectors and oscilloscopes allow us to interrogate the optical Sagnac effect directly by using the recently emerged methodologies of spatio-temporal intensity dynamics and DFT. We have shown in proof-of-principle experiments how the spatio-temporal dynamics approach can increase readout rates up to two orders of magnitude higher than commercially available options. The measurement configuration is also highly simplified, requiring only the use of a coupler for combining the counterpropagating pulses; accurate contemporization of the pulses becomes less of an issue. For experimental evaluation of the optical Sagnac effect, real-time spatio-temporal dynamics takes pulse relative motion as an advantage. The DFT approach also implies tolerable pulse separation.

Conventionally, in the case of synchronized repetition rates of counterpropagating pulses, the optical Sagnac effect is evaluated by measurement of the beat-note frequency of two combs using the RF spectrum analyzer, which are presented in [supplementary material 3](#). Apart from implications due to application of the actively stabilized delay line (from environmental effects) for contemporization of pulses and resulting phase and amplitude noise, the beat-note instabilities caused by the frequency drift of frequency combs of counterpropagating pulses significantly reduce the signal-to-noise ratio of the beat-note signal and resolution of the measurements. The resolution values obtained using DFT-based measurements were shown to be superior compared to conventional beat note measurements (see [supplementary material S3](#)). One of the reasons for this is that

the real-time measurement techniques eliminate the carrier-to-envelope offset frequency noise caused bias frequency drift.<sup>41</sup> In addition, no form of stabilization or even thermal isolation was applied. This can be attributed in part to the relatively short time scales investigated and to the high stability of the ultrafast laser (jitter  $< 0.8 \text{ ps}$ ).

The combination of the ultrashort pulse fiber laser design, together with the demonstrated signal processing approaches, presents significantly new and highly promising techniques of interrogating the optical Sagnac effect. The current laser configuration provides a rotation resolution of  $384 \mu\text{rad s}^{-1}$  in the spatio-temporal approach for  $N_{RT} = 10^4$  round trips and  $125 \mu\text{rad s}^{-1}$  for DFT analysis over 5000 round trips. Within the available range of platform rotation velocities, none of the presented techniques has demonstrated dead-band in optical Sagnac effect measurements. While more advanced and large-scale active laser configurations still offer better stability and accuracy, the results obtained using the relatively simple and compact bidirectional ultrafast laser hold a possibility to be further improved by more than an order of magnitude within the current laser design by increasing the number of round trips, or alternatively, by using a resonator of a larger scale. Extension of the laser cavity can lead to highly nontrivial pulse dynamics, as indicated by the observed deviation of the behavior of the studied laser from the linear Sagnac approximation. This was also confirmed in different context of achieving ultralong cavity operation.<sup>42,43</sup> The general methods proposed here can be applied in various applications beyond rotational sensing, helping to reveal the underlying physics of bidirectional ultrafast lasers. Currently, none of the existing theoretical models is capable to completely describe the dynamics of the interaction between counterpropagating solitons and their dispersive waves inside the bidirectional ultrafast fiber lasers, particularly, in the saturable absorber or their nonlocal interaction in the gain medium. Our further plans include development of such a numerical model to analyze pulse dynamics in the rotating cavity, which we have initiated while the current paper had been submitted and been undergoing the review process.<sup>44</sup>

Undoubtedly, the demonstrated resolution of demonstrated real-time measurement methodologies using the bidirectional ultrafast fiber laser is significantly lower than the one used in large ring laser gyroscopes ( $\sim 10^{-11} \text{ rad s}^{-1}$ ) and, therefore, restricts immediate application in seismic and gravitational wave detection within the demonstrated sensor concept. The capabilities of presented real-time measurement techniques can be enhanced further by the improvement of direct detection electronic systems for signal analysis. In addition, we acknowledge that the presented laser platform is not free of deficiencies. In this work, we used a bidirectional mode-locked laser as a convenient and straightforward platform to generate and study dynamics of ultrashort pulses during cavity rotation. In fact, recent works on seismology and gyroscopy demonstrate high progress in development of interferometers based on telecommunication optical fiber cables,<sup>45</sup> passive ultrafast FOGs,<sup>46</sup> or microresonator gyroscopes.<sup>47–49</sup> Yet, the performance of modern optical gyroscopes is often limited not by intrinsic physical effects, but rather by the available measurement methodology. Recently, emerged techniques for the characterization of optical field and laser radiation, in particular,<sup>19–24,27–30</sup> clearly demonstrate the high potential of the above-mentioned state-of-the-art gyroscopes to

enhancing performance further by using the novel approaches and measurement methodology as demonstrated here. Although it remains a subject for further investigation, we anticipate that the availability of a new generation of measurement techniques will lead to the development of new technology solutions for the real-time optical Sagnac effect visualization and enable translation of the proposed methodology to the future commercial gyroscopes.

## V. METHODS

### A. Experimental setup

In the experiment, the laser setup is similar to that presented in Ref. 50 (see Fig. 1). The fiber laser has a ring cavity configuration. A 2-m Erbium-doped fiber (EDF) (Liekki Er30-4/125) is pumped via laser diode at 980 nm through the 980/1550 wavelength division multiplexer (WDM). The total cavity length is 13.5 m with a corresponding fundamental repetition rate of  $\sim 14.7$  MHz [Fig. 5(c)]. The ultrashort pulse formation is realized via hybrid mode-locking, that is, by using simultaneously nonlinear polarization evolution (NPE) and single-walled carbon nanotubes (SWNTs). The NPE, being a fast saturable absorber, is achieved by introducing a 6-m coiled polarizing (PZ) fiber (HB1550Z from Thorlabs) and a pair of polarization controllers (PC), one of which is driven electronically (EPC). The bow-tie geometry of the PZ fiber modifies the optical fiber refractive index and, therefore, creates a different cut-off wavelength and attenuation for the orthogonally polarized fiber modes. The extinction ratio between slow and fast polarization axes is  $\sim 30$  dB within the bandwidth of  $\sim 130$  nm around 1550 nm. The SWNT/polymer sample features a high modulation depth around 54%, nonsaturable losses of 46%, and a saturation intensity of  $58.8 \text{ MW cm}^{-2}$  [Fig. 5(d)]. The individual pulse parameters of each clockwise (CW) and counterclockwise (CCW) channels are demonstrated in Fig. 5 when the platform is at rest. The laser generates near transform-limited soliton pulses in both operation directions [Figs. 5(a) and 5(b)]. The output power levels at the clockwise and counterclockwise channels are around 1 mW, and the pulse duration is 790 and 570 fs, respectively [Fig. 5(a)]. These parameters have not changed with the laser platform rotation. Ultrashort pulses from both laser outputs passing through isolators are combined via a 3-dB coupler.

The evaluation of the optical Sagnac effect via real-time dynamics is realized using a 33 GHz real-time oscilloscope (Agilent DSOX93204A) and a 50-GHz fast photodetector (Finisar

XPDV2320R) with the minimum temporal sampling rate of the entire measurement system of  $\sim 12.5$  ps.

### B. Optical Sagnac effect scale factor

#### 1. Spatio-temporal dynamics analysis

The difference in inclinations between the clockwise and counterclockwise pulses [as in Fig. 1(b)] arises due to a difference in their round trip time, in turn resulting from a difference in their carrier frequencies. This intrinsic difference between the round trip times can be taken as an offset for our configuration. When the stage starts to rotate with the angular velocity  $\Omega$ , the optical Sagnac effect leads to a further change in the cavity condition for the counterpropagating beams. The additional frequency difference introduced by the optical Sagnac effect can be recast as an increment to the cavity round trip time difference,  $\delta T_{N_{RT}}$ , accrued after  $N_{RT}$  round trips as

$$\delta T_{N_{RT}} = \frac{1}{f_{rep}^2} \frac{4A\Omega N_{RT}}{\lambda L} \equiv \frac{\Omega}{S}. \quad (2)$$

Here,  $f_{rep}$  is the pulse repetition rate,  $\lambda$  is the laser central wavelength,  $A$  is the area of the ring laser, and  $L$  is the length of the laser cavity. The repetition rate  $f_{rep}$  here is  $\sim 14.7$  MHz, according to averaged measurements in Fig. 5(c); the difference in the repetition rates of counter propagating pulses is  $\sim 60$  Hz, which is more than 5 orders of magnitude smaller and can be neglected in Eq. (2). Here,  $S$  takes the notion of the scale factor, specifying the value of the temporal shift induced per angular rate. For the laser currently employed, the scale factor as obtained via Eq. (2) using unit conversion coefficients is  $0.214 \text{ (deg s}^{-1}\text{) ps}^{-1}$  such that the resolution  $S \cdot \delta t = 5.349 \text{ deg s}^{-1}$ , where we have taken  $L = 13.5 \text{ m}$ ,  $A = 0.304 \text{ m}^2$ ,  $N_{RT} = 1$ , and  $\delta T_{N_{RT}} = 25 \text{ ps}$ , which is equal to the temporal resolution limit of our measurement configuration  $\delta t_{res}$ . For a fixed laser configuration, the scale factor and, therefore, resolution can be further increased by observing the relative temporal shift between the clockwise and counterclockwise pulses after several round trips (i.e., for  $N_{RT} \gg 1$ ). When using storage oscilloscopes, the recorded number of round trips can be as large as  $\sim 3.96 \times 10^5$ , thus increasing the resolution of the optical Sagnac effect measurements by the same order.

#### 2. DFT analysis

The sliding of the spectral fringes in the interference pattern of combined pulses [Fig. 4(b)] is caused by the infinitesimal drifting

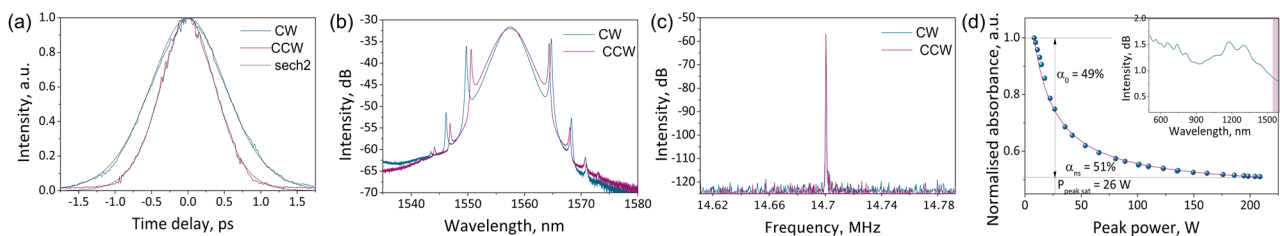


**FIG. 5.** Laser output characteristics for clockwise (CW) and counterclockwise (CCW) channels. (a) Autocorrelation traces. (b) Output spectra. (c) RF spectrum of the fundamental repetition rate. (d) Saturation behavior of SWNTs. Inset: linear absorption spectrum of SWNTs.

relative phase of combined pulses. Analogous to the above mentioned case, the tilt of the modulation pattern is referred to as the bias offset. The optical Sagnac effect introduces an additional change in optical path lengths for counterpropagating pulses, causing a further change in their carrier frequencies and, therefore, their relative phase when combined. In the ultrafast bidirectional laser, the phase change due to the optical Sagnac effect  $\phi = 8\pi AN_{RT}\Omega/(\lambda Lf_{rep})$  results in a change in the CEO. Conventionally, the CEO frequency was analyzed using beat-note measurements. The CEO of a complex of two pulses can be converted to a phase value as  $\phi = 2\pi\delta\nu/\Delta\nu$ , where  $\Delta\nu$  is the frequency of spectral modulation of the interference pattern of the individual single-shot spectrum and  $\delta\nu$  is the instantaneous CEO. The frequency of spectral modulation over consecutive round trips [along the white dashed line in Fig. 4(b)]  $f_{mod}$  over  $N_{RT}$  round trips can be estimated, analogous to Eq. (2), as

$$f_{mod} = \frac{f_{rep}\delta\nu}{\Delta\nu} = \frac{4AN_{RT}}{\lambda Lf_{rep}}\Omega \equiv \frac{\Omega}{S_{DFT}}. \quad (3)$$

Here,  $R$  is the radius of the rotational platform with a coiled laser setup. When the optical Sagnac effect is analyzed using the DFT technique, the scale factor  $S_{DFT}$  is defined by the induced frequency shift in spectral modulation over round trips per angular rate. With  $N_{RT} = 1$ , the scale factor  $S_{DFT}$  is 58 kHz/(deg s<sup>-1</sup>).

## SUPPLEMENTARY MATERIAL

See [supplementary material](#) for detailed description of real-time spatio-temporal and dispersive fourier transform measurement techniques; optical Sagnac assessment via beat-note frequency measurements; stability of scale factor; and ultrafast signal processing.

## ACKNOWLEDGMENTS

M.C. acknowledges the support of the Royal Academy of Engineering and Global Challenges Research Fund. S.K.T. acknowledges the support by the Russian Science Foundation (Grant No. 17-72-30006). The work of S.S. was supported by the Project H2020-MSCA-COFUND-MULTIPLY.

## REFERENCES

- <sup>1</sup>J. Belfi, N. Beverini, F. Bosi, G. Carelli, D. Cuccato, G. De Luca, A. Di Virgilio, A. Gebauer, E. Maccioni, A. Ortolan *et al.*, "Deep underground rotation measurements: GINGERino ring laser gyroscope in Gran Sasso," *Rev. Sci. Instrum.* **88**, 034502 (2017).
- <sup>2</sup>H. Igel, A. Cochard, J. Wassermann, A. Flaws, U. Schreiber, A. Velikosevtsev, and N. P. Dinh, "Broad-band observations of earthquake-induced rotational ground motions," *Geophys. J. Int.* **168**, 182–196 (2007).
- <sup>3</sup>C. Hadziioannou, P. Gaebler, U. Schreiber, J. Wassermann, and H. Igel, "Examining ambient noise using colocated measurements of rotational and translational motion," *J. Seismol.* **16**, 787–796 (2012).
- <sup>4</sup>K. U. Schreiber, T. Klügel, J.-P. R. Wells, R. B. Hurst, and A. Gebauer, "How to detect the Chandler and the annual wobble of the Earth with a large ring laser gyroscope," *Phys. Rev. Lett.* **107**, 173904 (2011).
- <sup>5</sup>I. P. Prikhodko, B. Bearss, C. Merritt, J. Bergeron, and C. Blackmer, "Towards self-navigating cars using MEMS IMU: Challenges and opportunities," in *2018 IEEE International Symposium on Inertial Sensors and Systems (INERTIAL)* (IEEE, 2018), pp. 1–4.
- <sup>6</sup>H. D. Escobar-Alvarez, N. Johnson, T. Hebble, K. Klingebiel, S. A. Quintero, J. Regenstein, and N. A. Browning, "R-ADVANCE: Rapid adaptive prediction

- for vision-based autonomous navigation, control, and evasion," *J. Field Rob.* **35**, 91–100 (2018).
- <sup>7</sup>H. C. Lefevre, *The Fiber-Optic Gyroscope* (Artech House, 2014).
- <sup>8</sup>S. Chao, W. L. Lim, and J. A. Hammond, "Lock-in growth in a ring laser gyro," in *Physics of Optical Ring Gyros* (International Society for Optics and Photonics, 1984), pp. 50–57.
- <sup>9</sup>D. Loukianov and N. A. T. Organization, *Optical Gyros and Their Application (Gyroscopes Optiques Et Leurs Applications)* (NATO Research and Technology Organization, Neuilly-Sur-Seine, France 1999), No. RTO-AG-339.
- <sup>10</sup>K. U. Schreiber and J.-P. R. Wells, "Large ring lasers for rotation sensing," *Rev. Sci. Instrum.* **84**, 041101 (2013).
- <sup>11</sup>P. Hansen, L. Eskildsen, J. Stentz, T. Strasser, J. Judkins, J. DeMarco, R. Pedrazzani, and D. DiGiovanni, "Rayleigh scattering limitations in distributed Raman pre-amplifiers," *IEEE Photonics Technol. Lett.* **10**, 159–161 (1998).
- <sup>12</sup>R. L. Fork, "Generation of optical pulses shorter than 0.1 psec by colliding pulse mode locking," *Appl. Phys. Lett.* **38**, 671 (1981).
- <sup>13</sup>F. Salin, P. Grangier, P. Georges, G. Le Saux, and A. Brun, "Nonreciprocal phase shifts in a femtosecond dye laser," *Opt. Lett.* **15**, 906–908 (1990).
- <sup>14</sup>N. Buholz and M. Chodorow, "Acoustic wave amplitude modulation of a multimode ring laser," *IEEE J. Quantum Electron.* **3**, 235 (1967).
- <sup>15</sup>J. Chesnoy, "Picosecond gyrolaser," *Opt. Lett.* **14**, 990–992 (1989).
- <sup>16</sup>A. A. Krylov, D. S. Chernykh, and E. D. Obratsova, "Gyroscopic effect detection in the colliding-pulse hybridly mode-locked erbium-doped all-fiber ring soliton laser," *Opt. Lett.* **42**, 2439–2442 (2017).
- <sup>17</sup>J. Hendrie, M. Lenzner, H. Afkhamiardakani, J. C. Diels, and L. Arissian, "Impact of resonant dispersion on the sensitivity of intracavity phase interferometry and laser gyros," *Opt. Express* **24**, 30402–30410 (2016).
- <sup>18</sup>E. Turitsyna, S. Smirnov, S. Sugavanam, N. Tarasov, X. Shu, S. Babin, E. Podivilov, D. Churkin, G. Falkovich, and S. Turitsyn, "The laminar-turbulent transition in a fibre laser," *Nat. Photonics* **7**, 783–786 (2013).
- <sup>19</sup>D. Churkin, S. Sugavanam, N. Tarasov, S. Khorev, S. V. Smirnov, S. M. Kobtsev, and S. K. Turitsyn, "Stochasticity, periodicity and localized light structures in partially mode-locked fibre lasers," *Nat. Commun.* **6**, 7004 (2015).
- <sup>20</sup>S. Sugavanam, N. Tarasov, and D. V. Churkin, "Real-time intensity domain characterization of fibre lasers using spatio-temporal dynamics," *Appl. Sci.* **6**, 65 (2016).
- <sup>21</sup>N. Tarasov, S. Sugavanam, and D. Churkin, "Spatio-temporal generation regimes in quasi-CW Raman fiber lasers," *Opt. Express* **23**, 24189–24194 (2015).
- <sup>22</sup>J. Peng, N. Tarasov, S. Sugavanam, and D. Churkin, "Rogue waves generation via nonlinear soliton collision in multiple-soliton state of a mode-locked fiber laser," *Opt. Express* **24**, 21256–21263 (2016).
- <sup>23</sup>J. M. Dudley, F. Dias, M. Erkintalo, and G. Genty, "Instabilities, breathers and rogue waves in optics," *Nat. Photonics* **8**, 755 (2014).
- <sup>24</sup>J. Peng, M. Sorokina, S. Sugavanam, N. Tarasov, D. V. Churkin, S. K. Turitsyn, and H. Zeng, "Real-time observation of dissipative soliton formation in nonlinear polarization rotation mode-locked fibre lasers," *Commun. Phys.* **1**, 20 (2018).
- <sup>25</sup>P. Kelkar, F. Coppinger, A. Bhushan, and B. Jalali, "Time-domain optical sensing," *Electron. Lett.* **35**, 1661–1662 (1999).
- <sup>26</sup>K. Goda, D. R. Solli, K. K. Tsia, and B. Jalali, "Theory of amplified dispersive Fourier transformation," *Phys. Rev. A* **80**, 043821 (2009).
- <sup>27</sup>K. Goda and B. Jalali, "Dispersive fourier transformation for fast continuous single-shot measurements," *Nat. Photonics* **7**, 102–112 (2013).
- <sup>28</sup>A. F. J. Runge, C. Agueraray, N. G. R. Broderick, and M. Erkintalo, "Coherence and shot-to-shot spectral fluctuations in noise-like ultrafast fiber lasers," *Opt. Lett.* **38**, 4327–4330 (2013).
- <sup>29</sup>A. F. J. Runge, N. G. R. Broderick, and M. Erkintalo, "Observation of soliton explosions in a passively mode-locked fiber laser," *Optica* **2**, 36–39 (2015).
- <sup>30</sup>G. Herink, B. Jalali, C. Ropers, and D. Solli, "Resolving the build-up of femtosecond mode-locking with single-shot spectroscopy at 90 MHz frame rate," *Nat. Photonics* **10**, 321–326 (2016).
- <sup>31</sup>H. J. Arditty and H. C. Lefevre, "Sagnac effect in fiber gyroscopes," *Opt. Lett.* **6**, 401–403 (1981).

- <sup>32</sup>S. Sugavanam, S. Fabbri, S. T. Le, I. Lobach, S. Kablukov, S. Khorev, and D. Churkin, "Real-time high-resolution heterodyne-based measurements of spectral dynamics in fibre lasers," *Sci. Rep.* **6**, 23152 (2016).
- <sup>33</sup>N. Smith and N. Doran, "Picosecond soliton transmission using concatenated nonlinear optical loop-mirror intensity filters," *J. Opt. Soc. Am. B* **12**, 1117–1125 (1995).
- <sup>34</sup>I. Gabitov, D. D. Holm, and B. P. Luce, "Low-noise picosecond soliton transmission by use of concatenated nonlinear amplifying loop mirrors," *J. Opt. Soc. Am. B* **14**, 1850–1855 (1997).
- <sup>35</sup>See <https://www.nxp.com/products/sensors/motion-sensors> for Motion sensors, 2019; accessed 24 October 2019.
- <sup>36</sup>J. Y. Liu, "High bandwidth coriolis vibratory gyroscope (CVG) with *in-situ* bias self-calibration," U.S. patent 9,534,897 (3 January 2017).
- <sup>37</sup>M. Yoshizawa and T. Kobayashi, "Experimental and theoretical studies on colliding pulse mode locking," *IEEE J. Quantum Electron.* **20**, 797–803 (1984).
- <sup>38</sup>S. Chin, V. Francois, J. Watson, and C. Delisle, "Spectral modulation of two coherently separated femtosecond laser pulses," *Appl. Opt.* **31**, 3383–3384 (1992).
- <sup>39</sup>B. Boashash, *Time-Frequency Signal Analysis and Processing: A Comprehensive Reference* (Academic Press, 2015).
- <sup>40</sup>B. Y. Kim, J. B. Hong, Y. B. Yeo, and B. W. Lee, "Fiber laser gyroscope with phase sensitive detection," U.S. patent 6,377,351 (23 April 2002).
- <sup>41</sup>J. Kim and Y. Song, "Ultralow-noise mode-locked fiber lasers and frequency combs: Principles, status, and applications," *Adv. Opt. Photonics* **8**, 465–540 (2016).
- <sup>42</sup>S. Kobtsev, S. Kukarin, and Y. Fedotov, "Ultra-low repetition rate mode-locked fiber laser with high-energy pulses," *Opt. Express* **16**, 21936–21941 (2008).
- <sup>43</sup>K. Kieu and M. Mansuripur, "All-fiber bidirectional passively mode-locked ring laser," *Opt. Lett.* **33**, 64–66 (2008).
- <sup>44</sup>I. S. Kudelin, S. Sugavanam, and M. Chernysheva, "Build-up of bidirectional ultrashort pulse laser generation: From Q-switched instabilities to mode-locking," in *The European Conference on Lasers and Electro-Optics* (Optical Society of America, 2019), p. cj\_7\_1.
- <sup>45</sup>G. Marra, C. Clivati, R. Lockett, A. Tampellini, J. Kronjäger, L. Wright, A. Mura, F. Levi, S. Robinson, A. Xuereb *et al.*, "Ultrastable laser interferometry for earthquake detection with terrestrial and submarine cables," *Science* **361**, 486–490 (2018).
- <sup>46</sup>K. Khanh, "All-ber bidirectional synchronously pumped ultrafast ring oscillator for precision sensing," U.S. patent application WO2016190913A2 (filed 4 April 2017).
- <sup>47</sup>J. Silver, L. D. Bino, and P. Del'Haye, "A nonlinear enhanced microresonator gyroscope," in *Conference on Lasers and Electro-Optics (CLEO)* (Optical Society of America, 2017), OSA Technical Digest, paper SM1M.2.
- <sup>48</sup>W. Liang, V. S. Ilchenko, A. A. Savchenkov, E. Dale, D. Eliyahu, A. B. Matsko, and L. Maleki, "Resonant microphotonic gyroscope," *Optica* **4**, 114–117 (2017).
- <sup>49</sup>S. Gundavarapu, G. M. Brodnik, M. Puckett, T. Huffman, D. Bose, R. Behunin, J. Wu, T. Qiu, C. Pinho, N. Chauhan *et al.*, "Sub-Hertz fundamental linewidth photonic integrated Brillouin laser," *Nat. Photonics* **13**, 60–67 (2019).
- <sup>50</sup>M. Chernysheva, M. A. Araimi, H. Khashi, R. Arif, S. V. Sergeyev, and A. Rozhin, "Isolator-free switchable uni- and bidirectional hybrid mode-locked erbium-doped fiber laser," *Opt. Express* **24**, 15721–15729 (2016).